Structure determination of $Pt_3Ti(111)$ by automated tensor LEED

1993 J. Phys.: Condens. Matter 5 4585

(http://iopscience.iop.org/0953-8984/5/27/003)

J. Phys.: Condens. Matter 5 (1993) 4585–4594. Printed in the UK

Structure determination of $Pt_3Ti(111)$ by automated tensor LEED

Wenhua Chen†, Jan A K Paul†‖, Angelo Barbieri‡, Michel A Van Hove‡, Steve Cameron§ and Daniel J Dwyer§¶

† Physics III, Royal Institute of Technology, S-100 44 Stockholm, Sweden
‡ Materials Sciences Division, Lawrence Berkeley Laboratory, Berkeley, CA 94720, USA
§ EXXON Research and Engineering Co., Route 22E, Annandale, NJ 08801, USA

Received 25 February 1993

Abstract. An analysis of low-energy electron diffraction (LEED) I–V spectra from the clean $Pt_3Ti(111)$ surface was performed by comparing measured intensities with data calculated using an automated tensor LEED program, which employs a directed search optimization procedure. It was found that the topmost layer is pure Pt and that the other layers have the bulk composition. The first and second interlayer spacings are 2.23 ± 0.03 Å and 2.21 ± 0.03 Å respectively, corresponding to a contraction of 0.9% and 1.8% of the bulk value. The perpendicular buckling is 0.04 Å ±0.05 Å in the top layer and 0.15 Å ±0.04 Å in the second layer. The results are in full accordance with previous investigations of the physical and chemical properties of this surface.

1. Introduction

Titania-supported platinum is a well known catalyst for the synthesis of methane from CO/H_2 [1]. Prolonged exposures to a reducing atmosphere at elevated temperatures leads to large dispersion changes in the catalyst. This is one of the effects commonly referred to as the strong metal support interaction (SMSI) [1]. Phase analyses also reveal the presence of Pt_3Ti, an ordered bimetallic alloy, under these conditions [2]. The catalytic importance of this phase is not known but it has motivated us to investigate the physical and chemical properties of $Pt_3Ti(111)$. The ordered alloy grows in the Cu_3Au lattice with a lattice constant of 3.906 Å [3]. Single-crystal surfaces of this alloy have been investigated by several methods including a low-energy electron diffraction (LEED) I–V characterization of the (100) surface [3–10].

All (111) planes of Pt_3Ti have stoichiometric composition in the bulk, but earlier work, based on angle-resolved photoemission, ion scattering, and CO adsorption, has indicated that the surface is plantinum enriched [10]. Images from scanning tunnelling microscopy (STM) and further measurements of core level energies support this thesis [11]. The present study is related to this work and presents LEED measurements of the $Pt_3Ti(111)$ crystal.

‖ For correspondence.

¶ Present address: University of Maine at Orono, Laboratory for Surface Science and Technology, Orono, ME 04469-0107, USA.

0953-8984/93/274585+10$07.50

2. Materials and methods

2.1. Experimental details

The $Pt_3Ti(111)$ crystal was gold brazed to a tantalum foil which served as a resistive heater [4] and was cleaned by repeated cycles of sputtering and annealing [10]. Special attention was paid to the annealing temperature, 1100 K for 5 minutes, since this may affect the degree of surface diffusion. Cleanliness was verified with Auger electron spectroscopy. This procedure gave sharp circular LEED spots with low background intensity. The clean surface displays a p(2 × 2) pattern relative to the (1 × 1) pattern of pure Pt(111) [4, 10].

LEED $I-V$ intensities were measured with a videocamera interfaced to a Varian LEED optics with a freshly coated fluorescent screen [12]. Normal incidence was verified by comparing $I-V$ intensities of degenerate beams. We present in this work the averaged intensities of symmetrical beams after eliminating beams where the line of sight was obstructed by the sample holder. $I-V$ curves were recorded for the $(\frac{1}{2}0)$, $(0\frac{1}{2})$, $(\frac{1}{2}\frac{1}{2})$, (10), (01), and (11) beams. The incident intensity as a function of beam energy was measured both directly as the emission current at the gun and as the sum of the intensities of all diffracted beams and the sample-to-ground current. The $I-V$ curves have been corrected for variations in the incident current.

The limited range of the framegrabber, 256 intensity levels, made it necessary to measure the intense peaks of the (1 × 1) integer beams and the much weaker fractional beams with different amplification and dark level settings on the videocamera. The terminology 'integer' and 'fractional' beams refers to a Pt(111) p(1 × 1) surface. A third set of measurements was made to normalize the digitized pixel intensities. Measurements made with varying incident beam angles will be presented elsewhere [13].

2.2. Calculations

$Pt_3Ti(111)$ constitutes a complicated scattering system with a likely surface segregation on top of an ordered bulk alloy. The bulk unit cell contains three Pt atoms and one Ti atom and all bulk (111) planes have stoichiometric composition. However complicated, this structure can still be treated readily by a recently developed perturbative approach [14, 15], based on the tensor LEED (TLEED) theory [16, 17], and a numerical search algorithm. This new technique employs an automatic directed search optimization procedure which significantly reduces the computer time required for an entire structure determination, compared to traditional methods. It allows many structural parameters to be found simultaneously and highly asymmetric systems to be solved easily. The program contains subroutines based on the renormalized forward scattering method for stacking layers and the combined space method for forming composite layers [18–20]. The calculation starts from a reference structure, for instance the unrelaxed surface structure, for which the LEED wavefunction and the reflected $I-V$ spectra are calculated exactly. Subsequently related trial surface structures, relaxed versions of the reference structure, are generated by distorting the reference surface, i.e. displacing some of the atoms away from their position in the reference structure. The trial structures are compared with experiment and the structural parameters optimized. Once the best-fit surface structure is found, one can refine it by repeating the search using the best-fit geometry as a new reference structure. The agreement between measured and calculated intensity curves is measured by R-factors, which are also used to direct the automatic optimization search [20]. In this work, the geometries of surface layers are optimized by minimizing the Pendry R-factor R_P [20, 21]. The lower R_P, the better the structural model used. The R_2-factor was also used for comparison [20, 22].

The muffin-tin model was used for the phase-shift calculations. Atomic wavefunctions of isolated atoms were computed using fully relativistic calculations, and were used to obtain the muffin-tin potential of Pt_3Ti [23]. The muffin-tin radius of non-touching platinum spheres was set to 1.01 Å while that of titanium was chosen to make the potential equal on the Pt and Ti muffin-tin spheres [24]. Increasing the value of the muffin-tin radius of platinum slightly worsens the R-factor, but this does not modify the best-fit structure significantly [24]. The influence of the 'atom radius' was also addressed in recent band structure calculations [11]. Phase shifts were generated by solving the Dirac equation and subsequently averaging over the two values of the spin. Calculations were performed by using eight phase shifts. The effect of lattice thermal vibrations was taken into account through standard temperature corrections to the phase shifts [19]. The Debye temperature of platinum was set to 300 K, that of titanium to 600 K and no attempt was made to fit these temperatures. In the course of calculation, the complex inner potential was initially chosen as $V_0 = -(10+5i)$eV, but the real part was subsequently optimized in the R-factor analysis.

3. Results

3.1. The structural models used in the calculation

The bulk Pt_3Ti has the Cu_3Au structure. Therefore, an ideal (111) surface of this crystal should have a layer stacking designated as ABCABC... and all layers should be identical with three Pt atoms and one Ti atom per unit cell; the Ti atoms reside on a (2×2) superlattice. The experimentally observed LEED pattern shown in figure 1 indicates that the surface has the two-dimensional periodicity related to the bulk structure.

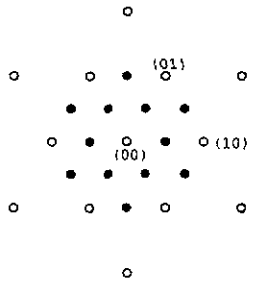

Figure 1. Schematic representation of the LEED pattern from the clean $Pt_3Ti(111)$ surface. The open circles correspond to the integer-order beams, while the filled circles represent some of the fractional-order beams.

Our previous study by x-ray photoelectron spectroscopy (XPS) and ion scattering spectroscopy (ISS) indicated that the clean surface of $Pt_3Ti(111)$ has a reconstructed structure where the first atomic layer is quasi-pure platinum [10]. Since the bulk termination structure of this crystal surface was proposed before [4], we started the calculation with bulk-like structures followed by Pt-enriched surface structures. Overall the following seven models were investigated:

(a) simple termination of the bulk lattice; denoted as 'bulk';

(b) termination of the bulk lattice with the top layer in a HCP-type layer stacking, i.e. CBCABC... instead of ABCABC...; denoted as 'bulk HCP';

(c) termination of the bulk lattice with broken symmetry in the top layer, i.e. the position of the Ti atom is exchanged with that of one of the Pt atoms; denoted as 'bulk BS';

(d) two Pt atoms and two Ti atoms per unit cell in the top layer, i.e. one of the three Pt atoms in the unit cell is replaced by a Ti atom; denoted as '0.5 Pt';

(e) one pure Pt layer on top of the bulk lattice; denoted as '1 Pt';

(f) one pure Pt layer as topmost layer, and two Pt atoms and two Ti atoms per unit cell as second outermost layer; denoted as '1 Pt+0.5 Pt';

(g) two pure Pt layers on top of the bulk lattice; denoted as '2 Pt'.

In these models, the surfaces of (a), (b), (e) and (g) preserve the symmetry of the simply terminated bulk structure (threefold rotation axis and three mirror planes), while the surfaces of (c), (d) and (f) break this symmetry.

3.2. The comparison of different models

The relative intensities among beams are significant in the determination of the surface structure. It turns out that at normal incidence the experimental intensities of the 'integer' beams are approximately ten times stronger than those of the 'fractional' beams. This is in contradiction with what is computed for models (a), (b), (c) and (d) where the calculated intensities of 'integer' beams are of the same order of magnitude as those of 'fractional' beams. The calculated intensities of the 'integer' beams are too strong relative to the 'fractional' beams for model (g) with an intensity ratio of about 40. A ratio of about 10 is calculated for models (e) and (f).

The above comparison of intensities among beams is sufficient to eliminate the possibility of the bulk termination structure (a) and the other four models (b), (c), (d) and (g). The R-factor analysis, which is insensitive to the overall intensity scale of each beam, also favours this conclusion. Table 1 shows the average R_P- and R_2-factors over the whole set of I–V curves for all the models considered. Notice that the best fit for the relaxed structures is obtained by exploring trial structures having the same symmetry of the corresponding reference structures (except for model (e), as explained later), and hence the number of fitting structural parameters is different for models with different symmetry. It is clear that the R_P-factors corresponding to the five models (a), (b), (c), (d), (g) are relatively high. Figure 2 shows the comparison of calculated and measured I–V spectra and relevant R_P-values for selected beams in different models tested. These comparisons are representative of results obtained for other beams at normal incidence.

Table 1. The average R_P- and R_2-factors over the whole set of I–V curves for all the models considered, before and after relaxation.

	Models	R_P, unrelaxed	R_P, relaxed	R_2, unrelaxed	R_2, relaxed
(a)	Bulk	0.71	0.58	0.49	0.26
(b)	Bulk HCP	0.81	0.69	0.50	0.29
(c)	Bulk BS	0.61	0.38	0.44	0.19
(d)	0.5 Pt	0.78	0.44	0.52	0.18
(e)	1 Pt	0.58	0.20	0.56	0.15
(f)	1 Pt+0.5 Pt	0.59	0.24	0.55	0.16
(g)	2 Pt	0.54	0.41	0.53	0.30

The computed intensities for the remaining two models (e) and (f) are consistent with the experimentally observed relative intensities of 'integer' and 'fractional' beams and these two models also give low R-factor values: $R_P = 0.24$ for (e) and $R_P = 0.22$ for (f) when the symmetry of the trial structures is restricted to that of the corresponding reference structure.

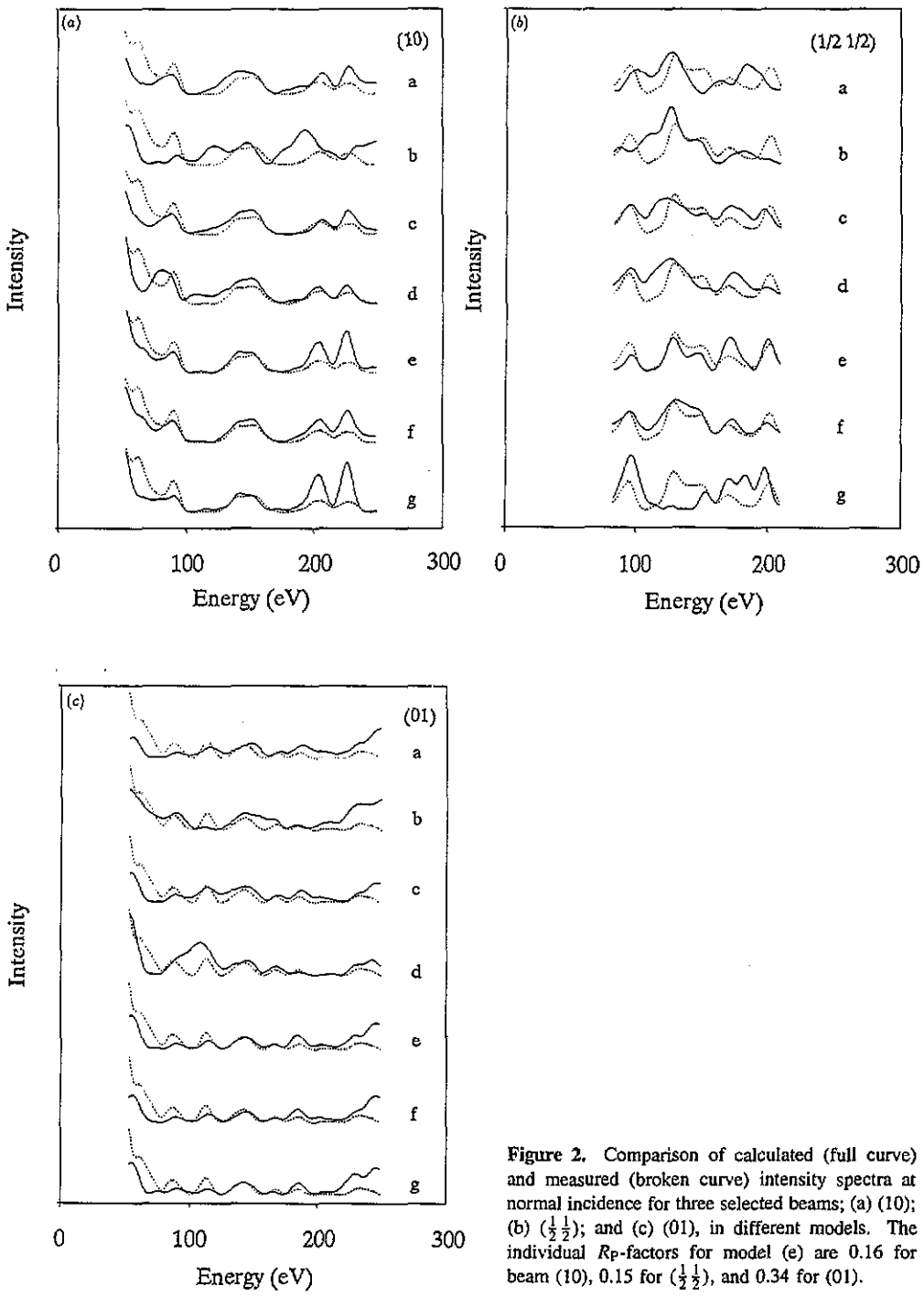

Figure 2. Comparison of calculated (full curve) and measured (broken curve) intensity spectra at normal incidence for three selected beams; (a) (10); (b) $(\frac{1}{2}\frac{1}{2})$; and (c) (01), in different models. The individual R_P-factors for model (e) are 0.16 for beam (10), 0.15 for $(\frac{1}{2}\frac{1}{2})$, and 0.34 for (01).

This small difference in R_P can be attributed however to the difference in the number of fitting parameters for these two structures due to their different symmetries (the symmetry is $p3m1$ for (e) and pm for (f)). Indeed, when using the same number of fitting parameters,

that is when the symmetry $p3m1$ of model (e) is relaxed to pm, R_P for model (e) was reduced from 0.24 to 0.22. In order to distinguish between models (e) and (f) we refined the search further by using the two best-fit geometries as new reference structures and by allowing both models to have the same number of fitting parameters. This decreases R_P from 0.22 to 0.20 for model (e) but increases R_P from 0.22 to 0.24 for model (f). This points to model (e) as the correct one, but we should stress that given the very close R-factor values of the two models it is not possible to exclude model (f) conclusively. Model (e) makes the $Pt_3Ti(111)$ surface Pt enriched, with one pure Pt layer on top of the bulk lattice.

3.3. Best-fit structure

So far, we have established that one pure Pt layer atop the bulk lattice structure gives the best agreement with experiment. Figure 3 shows that the top layer of this structure has two types of Pt atoms, corresponding to the different neighbours in the second atomic layer. One Pt atom per unit cell in the top layer contacts three Pt atoms of the second layer, and three Pt atoms per unit cell in the top layer contact two Pt atoms and one Ti atom of the second layer. This difference allows buckling and lateral displacements in several layers: we have fitted these quantities in the top two layers.

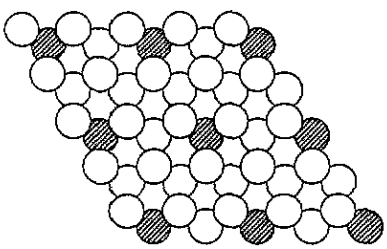

Figure 3. Schematic top view of best-fit structural model for the $Pt_3Ti(111)$ surface, showing the top two layers only. Ti atoms are hatched.

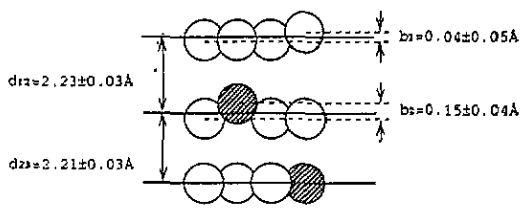

Figure 4. Schematic side view of best-fit structural model for the $Pt_3Ti(111)$ surface, with the surface at the top of figure. Ti atoms are hatched.

The refinement of this structure leads to the following structural parameters (figure 4): the buckling in the top layer is $b_1 = 0.04$ Å with the plane of the first type of Pt atoms (one per unit cell) displaced upwards and the plane of the second type of Pt atoms (three per unit cell) displaced downwards. The buckling in the second layer is $b_2 = 0.15$ Å with the plane of Ti atoms moved upwards and the plane of Pt atoms moved downwards. The bucklings in these two layers induce contractions of both the first interlayer and the second interlayer spacing by 0.02 Å and 0.04 Å, or 0.9% and 1.8% with respect to the bulk value of 2.25 Å, where the interlayer spacings are measured between average planes of the buckled layers, giving Pt and Ti atoms equal weights. There are also very small and probably insignificant, considering the respective error bars, lateral displacements of atoms in these two layers. In the top layer, the first type of Pt atoms (one per unit cell) have no lateral movements because of symmetry while the second type of Pt atoms (three per unit cell) move radially toward the Ti atoms of the second layer by 0.01 ± 0.05 Å. In the second layer the Pt atoms move laterally toward the Ti atoms of the third layer by 0.02 ± 0.10 Å.

The error bars for the structural parameters in figure 4, derived using Pendry's statistical estimate, are about ± 0.03 Å for the interlayer spacings, ± 0.05 Å for the buckling in the top layer and ± 0.04 Å for the buckling in the second layer. The optimized atomic

Table 2. Optimized atomic coordinates (Å) of the best-fit structural model for $Pt_3Ti(111)$ obtained by preserving the full symmetry $p3m1$ (x: perpendicular; y, z: parallel to the surface). The third-layer coordinates were not fitted but are reported here with the bulk repeat vector to give complete information about the structural model. The coordinates of the nth layer (for $n > 3$) are obtained by translating those of the $(n-1)$th layer by the bulk repeat vector.

Layer	x	y	z	Atom	Layer	x	y	z	Atom
1st	0.034	2.758	−1.592	Pt	3rd	4.503	2.758	1.592	Ti
	0.077	0.000	−1.585	Pt		4.503	1.379	−0.796	Pt
	0.077	1.373	0.793	Pt		4.503	−1.379	−0.796	Pt
	0.077	−1.373	0.793	Pt		4.503	0.000	1.592	Pt
2nd	2.180	0.000	0.000	Ti	Bulk repeat	2.252	0.000	−3.184	
	2.334	2.758	0.016	Pt	values				
	2.334	1.392	2.381	Pt					
	2.334	−1.392	2.381	Pt					

Table 3. Optimized atomic coordinates (Å) of the best-fit structural model for $Pt_3Ti(111)$ corresponding to complete relaxation of the symmetry (x: perpendicular; y, z: parallel to the surface). See caption of table 2 for third layer and bulk repeat vector. Error bars on the individual vertical coordinates of atoms in the first layer and of the Ti atom in the second layer are about ±0.05 Å, on the vertical coordinates of the remaining atoms in the second layer are about ±0.10 Å. Error bar on each individual lateral coordinate is about ±0.15 Å.

Layer	x	y	z	Atom	Layer	x	y	z	Atom
1st	0.037	2.921	−1.509	Pt	3rd	4.503	2.758	1.592	Ti
	0.038	0.123	−1.661	Pt		4.503	1.379	−0.796	Pt
	0.088	1.338	0.757	Pt		4.503	−1.379	−0.796	Pt
	0.061	−1.371	0.821	Pt		4.503	0.000	1.592	Pt
2nd	2.190	−0.060	−0.140	Ti	Bulk repeat	2.252	0.000	−3.184	
	2.352	2.614	0.093	Pt	values				
	2.307	1.299	2.441	Pt					
	2.301	−1.527	2.410	Pt					

coordinates corresponding to symmetry conserving displacements are listed in table 2 while those corresponding to a complete relaxation of the symmetry are listed in table 3.

Figure 5 presents the intensity curves for the above best-fit model and table 4 displays the R-factors corresponding to the different degrees of relaxation allowed in the fitting procedure for this model (the numbers in this table and table 1 are not directly comparable because some of them are obtained by using different reference structures). It is found that the perpendicular displacements of atoms in the two topmost layers reduce the R_P-factor significantly, but the perpendicular displacements of the atoms in the third layer and the lateral displacements of the atoms do not improve the R_P-value markedly.

4. Discussion

An analysis of LEED intensity profiles leads to the conclusion that the top atomic layer of the $Pt_3Ti(111)$ surface is pure platinum. This is in full agreement with our previous findings by XPS, ISS, and CO adsorption measurements [10]. We acknowledge the difficulty in establishing the stoichiometry of subsequent layers, due to the strong scattering of the topmost Pt layer, but no structure gives a better agreement with experimental data than the bulk 3:1 ratio between Pt and Ti. Spencer proposed, on the basis of the broken-bond model,

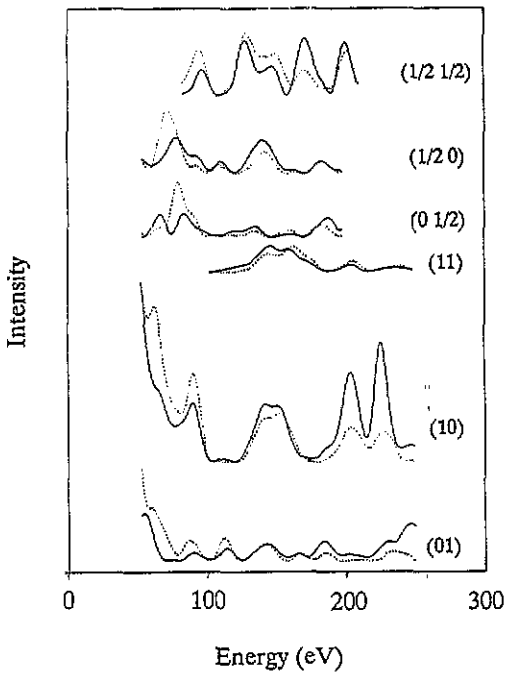

Figure 5. The intensity spectra for the best-fit structural model. Full and broken curves represent theoretical and experimental curves respectively.

Table 4. *R*-factors corresponding to the different degrees of relaxation allowed in the fitting procedure for the best-fit structural model. The numbers in parentheses are the number of structural parameters being fitted.

Symmetry	Degree of relaxation	R_P
*p*3*m*1 (0)	No relaxation	0.58
*p*3*m*1 (2)	Perpendicular for top layer	0.40
*p*3*m*1 (4)	Perpendicular for top two layers	0.25
*p*3*m*1 (6)	Perpendicular for top three layers	0.25
*p*3*m*1 (6)	Perpendicular and lateral for top two layers	0.25
pm (14)	Perpendicular and lateral for top two layers	0.20
*p*1 (24)	Perpendicular and lateral for top two layers	0.19

that the two factors controlling the thermodynamics of segregation in alloys are the strain energy and the surface free energy [25]. The strain energy originates from the mismatch of the sizes of the atoms, and the surface free energy comes from the bonding between atoms. For the Pt_3Ti alloy, the size of the Ti atom is smaller than the size of the Pt atom so that the strain energy does not favour the segregation of Ti atoms [26]. Moreover, there are no Ti–Ti bonds, and all titanium atoms are coordinated to 12 platinum atoms as nearest neighbours while the platinum atoms are coordinated to eight platinum atoms and four titanium atoms as nearest neighbours. Since the free energy of the Pt–Ti bond is larger than that of the Pt–Pt bond [25,27], the surface free energy will also not allow Ti atoms to occupy the surface. Indeed, calculations using thermodynamic data also suggested the segregation of platinum on the $Pt_3Ti(111)$ surface [25].

Physically, the primary mechanism of surface segregation is the diffusion of one component in an alloy from the bulk. The driving force for the segregation is the difference

in the chemical potentials between the surface and the bulk for this alloy [28]. When equilibrium is achieved, the minimization of the total free energy at a given temperature may result in some surface segregation to obtain thermodynamic equilibrium. The amount of segregation will depend on the equilibrium temperature of the bulk alloy.

5. Conclusions

The present work reports the structure of the clean $Pt_3Ti(111)$ surface as determined by LEED analysis. It reveals that the top layer is pure platinum and that other layers have the bulk Pt:Ti ratio 3:1. There is small contraction of 0.02 Å ± 0.03 Å for the first interlayer spacing and 0.04 Å ± 0.03 Å for the second interlayer spacing. It is also found that there is a small buckling in the top layer 0.04 Å ± 0.05 Å and larger buckling in the second layer 0.15 Å ± 0.04 Å. Atoms in the third layer have the bulk positions and the third interlayer spacing has the bulk value.

Acknowledgments

We gratefully acknowledge discussions with J Rudgren at the Royal Institute of Technology and P N Ross at the Lawrence Berkeley Laboratory. The crystal was provided by Dr Ross and the video–LEED system by Dr Hoffmann. This work was supported in part by the Swedish Technical Research Council and in part by the Director, Office of Energy Research, Office of Basic Energy Sciences, Materials Sciences Division of the US Department of Energy under Contract No DE-AC03-76SF00098.

References

[1] Baker R T K, Tauster S J and Dumesic J A (ed) 1986 *Strong-Metal-Support Interactions (ACS Symposium Series 298)* (Washington, DC: ACS)
[2] Beard B C and Ross P N 1986 *J. Phys. Chem.* **90** 6811
[3] Atrei A, Pedocchi L, Bardi U, Rovida G, Torrini M, Zanazzi E, Van Hove M A and Ross P N 1992 *Surf. Sci.* **261** 64
[4] Bardi U and Ross P N 1984 *Surf. Sci.* **146** L555
[5] Bardi U and Ross P N 1984 *J. Vac. Sci. Technol.* A **2** 1461
[6] Bardi U, Dahlgren D and Ross P N 1986 *J. Catal.* **100** 196
[7] Mehandru S P, Anderson A B and Ross P N 1986 *J. Catal.* **100** 210
[8] Cameron S D and Dwyer D J 1986 *Surf. Sci.* **176** L857
[9] Cameron S D and Dwyer D J 1987 *J. Vac. Sci. Technol.* A **5** 651
[10] Paul J, Cameron S D, Dwyer D J and Hoffmann F M 1986 *Surf. Sci.* **177** 121
[11] Chen W, Tillborg H, Severin L, Johansson B, Nilsson A, Mårtensson N, Göthelid M, Hammar M, Cameron S and Paul J 1993 *Phys. Rev.* B submitted
[12] Video–LEED analyser, Data-Quire Corporation, Stony Brook (1982)
[13] Chen W, Paul J, Cameron S, Dwyer D J and Hoffmann F M 1993 unpublished
[14] Rous P J, Van Hove M A and Somorjai G A 1990 *Surf. Sci.* **226** 15
[15] Van Hove M A, Moritz W, Over H, Rous P J, Wander A, Barbieri A, Materer N, Starke U and Somorjai G A 1993 *Surf. Sci. Rep.* at press
[16] Rous P J and Pendry J B 1989 *Surf. Sci.* **219** 355
[17] Rous P J and Pendry J B 1989 *Surf. Sci.* **219** 373
[18] Pendry J B 1974 *Low Energy Electron Diffraction* (New York: Academic)
[19] Van Hove M A and Tong S Y 1979 *Surface Crystallography by LEED* (Berlin: Springer)
[20] Van Hove M A, Weinberg W H and Chan C M 1986 *Low-Energy Electron Diffraction* (New York: Springer)

[21] Pendry J B 1980 *J. Phys. C: Solid State Phys.* **13** 937
[22] Van Hove M A, Tong S Y and Elconin M H 1977 *Surf. Sci.* **64** 85
[23] Loucks T L 1967 *Augmented Plane Wave Method* (New York: Benjamin)
[24] Starke U, Barbieri A, Materer N, Van Hove M A and Somorjai G A 1993 *Surf. Sci.* at press
[25] Spencer M S 1984 *Surf. Sci.* **145** 145
[26] Abraham F F, Tsai N H and Pound G M 1979 *Surf. Sci.* **83** 406
[27] Hultgren R, Orr R L, Anderson P D and Kelley K K 1963 *Selected Values of Thermodynamic Properties of Metals and Alloys* (New York: Wiley)
[28] Mazurowski J and Dowben P A 1990 *Surface Segregation Phenomena* ed P A Dowben and A Miller (Boca Raton, FL: Chemical Rubber Company)